

Gravitational waves from a dust disk around a Schwarzschild black hole

Hajime Sotani

*Research Institute for Science and Engineering, Waseda University, Okubo 3-4-1, Shinjuku, Tokyo 169-8555, Japan**

Motoyuki Saijo[†]

Laboratoire de l'Univers et de ses Théories, Observatoire de Paris, F-92195 Meudon Cedex, France

(Received 6 July 2005; Revised 22 May 2006; Accepted 15 June 2006)

We investigate gravitational waves from a dust disk around a Schwarzschild black hole to focus on whether we can extract any of its physical properties from a direct detection of gravitational waves. We adopt a black hole perturbation approach in a time domain, which is a satisfactory approximation to illustrate a dust disk in a supermassive black hole. We find that we can determine the radius of the disk by using the power spectrum of gravitational waves and that our method to extract the radius works for a disk of arbitrary density distribution. Therefore we believe a possibility exists for determining the radius of the disk from a direct observation of gravitational waves detected by the Laser Interferometer Space Antenna.

PACS numbers: 04.30.Db, 04.25.Nx, 04.70.-s

I. INTRODUCTION

Gravitational wave projects have been launched in many countries to explore a new world in gravitational physics, in astrophysics, and in cosmology. Nowadays, several ground-based laser interferometric gravitational wave detectors such as TAMA300, LIGO, GEO600, and VIRGO have been seeking for a direct detection of gravitational waves (See Ref. [1] for the current status of the worldwide network of gravitational wave detectors). The sensitive frequency for the ground-based interferometers is within the range of 10 – 1000 Hz. The representative sources of gravitational waves are the inspiral of binary systems composed of neutron stars and black holes, spinning neutron stars, and low-mass x-ray binaries [2]. There will be also a gravitational wave detector in space, Laser Interferometer Space Antenna (LISA). The sensitive frequency band in LISA is in the range of 10^{-4} – 10^{-1} Hz, and one of the representative gravitational wave sources this detector is studying is supermassive black holes whose masses are $M \sim 10^6$ – $10^9 M_\odot$. There is increasing evidence that a supermassive black hole exists at the center of every galaxy [3].

There is abundant observational evidence for dense gas in galactic nuclei [e.g., 3, 4]. For example, our galactic nuclei contains a $4 \times 10^6 M_\odot$ supermassive black hole surrounded by an $\sim 10^4 M_\odot$ molecular gas torus [e.g., 5]. Also the disruption of a compact star by a supermassive black hole spreads the gas in black hole spacetime [6, 7]. From a theoretical point of view, the tidal disruption of a star by a supermassive black hole has been studied in

Newtonian gravity [e.g., 8, 9, 10, 11, 12] and in post-Newtonian gravity [13], where the black hole is regarded as a point mass. There are also several studies of tidal disruption in a Schwarzschild black hole [14, 15] and in a Kerr black hole [16, 17, 18, 19]. In all cases, the fragments of the disrupted star are either swallowed by the supermassive black hole or following a highly eccentric orbits. There is also an indication, based on an observation, that a disk can form around a supermassive black hole [20].

Black hole perturbation approach is one of the satisfactory tools to illustrate gravitational waves from a compact star around a supermassive black hole. Many works have been published in post-Newtonian expansion [21], in numerical analysis [22] to compute gravitational waves from a test particle in a Kerr black hole. However all of the above works have been investigated in a Fourier domain, which means that the orbital time of the particle is infinite. The basic equations of gravitational waves are ordinary differential ones, but we have to treat “infinite” orbital time by restricting our orbit to a special one. There is another way of computing linearized Einstein equations: a time domain approach, which directly solves the basic equations in partially differential ones. The main advantages of this time domain approach are that we can impose an initial condition as an appropriate distribution of the compact object and that we can treat an arbitrary orbit of the particle in general. There are many studies in the field of time domain computation of the head-on collision of two black holes perturbatively [23, 24, 25], of black hole perturbation in Schwarzschild spacetime [26, 27, 28, 29, 30] and in Kerr spacetime [31, 32, 33, 34], of perturbation in spherical stars [35, 36, 37, 38, 39], of perturbation in nonrotating objects [40] and of perturbation in slowly rotating stars [41, 42].

Our purpose in this paper is to investigate whether we can extract any physical property of the disk around a supermassive black hole from gravitational waves. Several

*Electronic address: sotani@astro.auth.gr;

Present address: Department of Physics, Aristotle University of Thessaloniki, Thessaloniki 54124, Greece.

[†]Electronic address: ms1@maths.soton.ac.uk;

Present address: School of Mathematics, University of Southampton, Southampton SO17 1BJ, United Kingdom.

studies have investigated extracting physical properties of a tidally disrupted star in supermassive black holes [43, 44, 45, 46, 47]. When the disk is formed from tidal disruption of a star by a supermassive black hole, test particle approximation to illustrate the fragments is a satisfactory tool since the pressure gradient is no longer dominant [47]. Saijo and Nakamura [44, 45] investigated a tidally disrupted star falling into a black hole and found that we can extract the size of the star from the energy spectrum of gravitational waves. Although they investigated gravitational radiation in a Fourier domain, inappropriate description of the pre-disruption of the star, their Fourier domain approach does almost illustrate the picture of post-disruption appropriately since most gravitational waves are radiated at a quasi-normal ringing phase. Here we mainly focus on gravitational waves from a disrupted star around a supermassive black hole in a time domain to learn whether we can extract any physical property of a dust disk. We have to deal with two types of test particle orbit in our dust disk calculation due to the angular momentum depletion. Particles both plunging into and orbiting a Schwarzschild black in the same calculation. To perform the above situation from the computational point of view, time domain approach is quite easy to handle rather than Fourier domain one.

This paper is organized as follows. In Sec. II, we briefly describe the basic equations of gravitational waves from a test particle. In Sec. III, we demonstrate gravitational waves from a test particle in our developed code, comparing with well-known results in this field. In Sec. IV, we show gravitational waves from a dust disk around a Schwarzschild black hole. We summarize our paper in Sec. V. Throughout this paper, we use geometrized units $G = c = 1$, where G and c denote the gravitational constant and the speed of light, respectively, and the metric sign as $(-, +, +, +)$.

II. BLACK HOLE PERTURBATION APPROACH IN SCHWARZSCHILD SPACETIME

Here we describe the basic equations of gravitational waves in order to compute gravitational waves from a test particle around a Schwarzschild black hole.

First, we describe the motion of a test particle with a rest mass μ around a Schwarzschild black hole with a gravitational mass M . In this paper, we only consider the motion of a test particle in the equatorial plane. The motion is specified by giving the two parameters \tilde{E}_p and \tilde{L}_p in units of μ as

$$\tilde{E}_p = E_p/\mu, \quad \tilde{L}_p = L_p/\mu, \quad (2.1)$$

where E_p and L_p are the energy and the total angular momentum of a test particle observed at infinity, respectively. With these parameters, the equation of motion of

a test particle is described as

$$\frac{d^2 r_*}{dt^2} = \frac{1}{\tilde{E}_p^2} \left(1 - \frac{2M}{r}\right) \left[-\frac{M}{r^2} + \frac{\tilde{L}_p^2}{r^3} \left(1 - \frac{3M}{r}\right)\right], \quad (2.2)$$

$$\frac{d\phi}{dt} = \frac{1}{r^2} \left(1 - \frac{2M}{r}\right) \frac{\tilde{L}_p}{\tilde{E}_p}, \quad (2.3)$$

where $r_* = r + 2M \ln(r/2M - 1)$ is the tortoise coordinate. We also introduce the effective potential \tilde{V}_p by integrating the radial motion of a test particle (Eq. [2.2]) as

$$\left(\frac{dr_*}{dt}\right)^2 = 1 - \left(\frac{\tilde{V}_p(r)}{\tilde{E}_p}\right)^2, \quad (2.4)$$

$$\tilde{V}_p(r) = \sqrt{\left(1 - \frac{2M}{r}\right) \left(1 + \frac{\tilde{L}_p^2}{r^2}\right)}. \quad (2.5)$$

The potential \tilde{V}_p has a local minimum when $\tilde{L}_p \geq 2\sqrt{3}M$ at the radius

$$r = \frac{\tilde{L}_p}{2M} \left(\tilde{L}_p + \sqrt{\tilde{L}_p^2 - 12M^2}\right), \quad (2.6)$$

where the particle has a stable circular orbit.

Next, we describe the basic equations of gravitational waves. These equations are obtained by linearizing the Einstein equations in Schwarzschild spacetime called Regge-Wheeler equations for odd parity [48] and Zerilli equations for even parity [49]. Note that we can only treat odd and even parity separately in the nature of spherical symmetric background spacetime.

The radial wave function of gravitational waves obeys Regge-Wheeler-Zerilli equations as

$$\left[-\frac{\partial^2}{\partial t^2} + \frac{\partial^2}{\partial r_*^2} - V_l(r)^{(\text{odd/even})}\right] \Psi_{lm}^{(\text{odd/even})}(t, r) = S_{lm}^{(\text{odd/even})}(t, r), \quad (2.7)$$

where $\Psi_{lm}^{(\text{odd/even})}$, $S_{lm}^{(\text{odd/even})}$, $V_l^{(\text{odd/even})}$ is the radial wave function, source term, and effective potential of gravitational waves, respectively. The effective potentials for odd and even parities are given by

$$V_l^{(\text{odd})} = \frac{2f}{r^2} \left(\lambda + 1 - \frac{3M}{r}\right), \quad (2.8)$$

$$V_l^{(\text{even})} = \frac{2f(\lambda^2(\lambda+1)r^3 + 3M\lambda^2r^2 + 9M^2\lambda r + 9M^3)}{r^5\Lambda^2}, \quad (2.9)$$

where $f \equiv 1 - 2M/r$, $\Lambda \equiv \lambda + 3M/r$, and $\lambda \equiv (l+2)(l-1)/2$. The source terms are constructed from the energy

momentum tensor of a test particle as

$$S_{lm}^{(\text{odd})} = -\frac{8\pi r f}{\sqrt{2\lambda(\lambda+1)}} \left[\frac{d}{dr} (f D_{lm}) - \frac{\sqrt{2\lambda} f}{r} Q_{lm} \right], \quad (2.10)$$

$$\begin{aligned} S_{lm}^{(\text{even})} = & \frac{8\pi}{(\lambda+1)\Lambda} \left[r^2 f \left(f^2 \frac{\partial}{\partial r} (f^{-2} A_{lm}^{(0)}) - \frac{\partial}{\partial r} (f^2 A_{lm}) \right) \right. \\ & + r f^2 (\Lambda - f) A_{lm} + \sqrt{2} r f^2 G_{lm} \\ & \left. - \frac{1}{r\Lambda} [\lambda(\lambda-1)r^2 + (4\lambda-9)Mr + 15M^2] A_{lm}^{(0)} \right] \\ & + \frac{16\pi r f^2}{\Lambda\sqrt{\lambda+1}} B_{lm} - \frac{16\pi r f}{\sqrt{2\lambda(\lambda+1)}} F_{lm}, \quad (2.11) \end{aligned}$$

where

$$A_{lm}^{(0)} = \mu\gamma f^2 \frac{\delta(r-\hat{R})}{r^2} \bar{Y}_{lm}(\hat{\Omega}), \quad (2.12)$$

$$A_{lm} = \mu\gamma \left(\frac{d\hat{R}}{dt} \right)^2 \frac{\delta(r-\hat{R})}{(r-2M)^2} \bar{Y}_{lm}(\hat{\Omega}), \quad (2.13)$$

$$B_{lm} = \mu\gamma \sqrt{\frac{1}{\lambda+1}} \frac{d\hat{R}}{dt} \frac{\delta(r-\hat{R})}{r-2M} \frac{d\bar{Y}_{lm}(\hat{\Omega})}{dt}, \quad (2.14)$$

$$D_{lm} = \frac{i\mu\gamma\delta(r-\hat{R})}{2\sqrt{2\lambda(\lambda+1)}} \left(\frac{d\hat{\Phi}}{dt} \right)^2 \bar{X}_{lm}(\hat{\Omega}), \quad (2.15)$$

$$F_{lm} = -\frac{\mu\gamma\delta(r-\hat{R})}{2\sqrt{2\lambda(\lambda+1)}} \left(\frac{d\hat{\Phi}}{dt} \right)^2 \bar{W}_{lm}(\hat{\Omega}), \quad (2.16)$$

$$G_{lm} = \frac{\mu\gamma}{\sqrt{2}} \delta(r-\hat{R}) \left(\frac{d\hat{\Phi}}{dt} \right)^2 \bar{Y}_{lm}(\hat{\Omega}), \quad (2.17)$$

$$Q_{lm} = i\mu\gamma \sqrt{\frac{1}{\lambda(\lambda+1)}} \frac{\delta(r-\hat{R})}{r-2M} \frac{d\hat{R}}{dt} \frac{d\hat{\Phi}}{dt} \frac{\partial Y_{lm}(\hat{\Omega})}{\partial \theta}. \quad (2.18)$$

Note that $A_{lm}^{(0)}$, A_{lm} , B_{lm} , D_{lm} , F_{lm} , G_{lm} , and Q_{lm} are the coefficients expanded in tensor harmonics [49]. Note also that $\gamma \equiv dt/d\tau = \tilde{E}_p/(1-2M/r)$, where τ is a proper time of the particle. $X^i(t) = (\hat{R}(t), \hat{\Omega}(t))$ is the location of a particle, where $\hat{\Omega} = (\pi/2, \hat{\Phi}(t))$. Also a quantity \bar{A} represents the complex conjugate of a quantity A . The functions X_{lm} and W_{lm} are the tensorial part of tensor harmonics defined by

$$X_{lm} = 2\partial_\phi(\partial_\theta - \cot\theta)Y_{lm}, \quad (2.19)$$

$$W_{lm} = \left(\partial_\theta^2 - \cot\theta\partial_\theta - \frac{\partial_\phi^2}{\sin^2\theta} \right) Y_{lm}. \quad (2.20)$$

Finally, we mention the relationship between the radial wave function and the perturbed metric in the wave zone.

It is written as [Eq. (3.1) of Ref. [28]]

$$\begin{aligned} h_+ - ih_\times = & \frac{1}{2r} \sum_{l,m} \sqrt{\frac{(l+2)!}{(l-2)!}} {}_{-2}Y_{lm}(\theta, \varphi) \\ & \times \left(\Psi_{lm}^{(\text{even})} - 2i \int^t dt' \Psi_{lm}^{(\text{odd})} \right), \quad (2.21) \end{aligned}$$

where spin-weighted spherical harmonics ${}_{-2}Y_{lm}(\theta, \varphi)$ is defined by

$${}_{-2}Y_{lm}(\theta, \varphi) = \frac{1}{2\sqrt{\lambda(\lambda+1)}} \left(W_{lm} - \frac{i}{\sin\theta} X_{lm} \right). \quad (2.22)$$

The energy flux (dE_{gw}/dt) of gravitational waves at the wave zone is also given by [Eq. (B.26) of Ref. [28]]

$$\frac{dE_{\text{gw}}}{dt} = \frac{1}{64\pi} \sum_{l,m} \frac{(l+2)!}{(l-2)!} \left[\left| \frac{\partial}{\partial t} \Psi_{lm}^{(\text{even})} \right|^2 + 4 \left| \Psi_{lm}^{(\text{odd})} \right|^2 \right]. \quad (2.23)$$

III. GRAVITATIONAL WAVES FROM A TEST PARTICLE IN SCHWARZSCHILD SPACETIME

Here we compute gravitational waves from a test particle in Schwarzschild spacetime. We use a time domain approach to solve Eq. (2.7). In order to test our newly developed code, we compare our results in two cases with well-known semi-analytical results. One is gravitational waves from a particle in a circular orbit around a Schwarzschild black hole, which has been studied up to the 5.5 post-Newtonian order [50]. The other is gravitational waves from a particle with a radial in-fall into a Schwarzschild black hole in a Fourier domain [51].

We set the initial condition of the radial wave function as

$$\Psi_{lm}^{(\text{odd/even})} \Big|_{t=0} = 0, \quad \frac{\partial \Psi_{lm}^{(\text{odd/even})}}{\partial t} \Big|_{t=0} = 0, \quad (3.1)$$

with the boundary condition that there is no incoming wave to our system. Namely, we impose the outgoing wave boundary condition for the radial wave function at horizon and at a spatial infinity as

$$\left(\frac{\partial}{\partial t} + \frac{\partial}{\partial r_*} \right) \Psi_{lm}^{(\text{odd/even})} = 0 \quad \text{at} \quad r_* = r_*^{\text{in}}, \quad (3.2)$$

$$\left(\frac{\partial}{\partial t} - \frac{\partial}{\partial r_*} \right) \Psi_{lm}^{(\text{odd/even})} = 0 \quad \text{at} \quad r_* = r_*^{\text{out}}, \quad (3.3)$$

where r_*^{in} and r_*^{out} are the inner and outer edge of the computational grid. In practice Eqs. (3.2) and (3.3) are

written as

$$\begin{aligned} \Psi_{lm}^{(\text{odd/even})}(t + \Delta t, r_*^{\text{in}}) &= \left(1 - \frac{\Delta t}{\Delta r_*}\right) \Psi_{lm}^{(\text{odd/even})}(t, r_*^{\text{in}}) \\ &+ \frac{\Delta t}{\Delta r_*} \Psi_{lm}^{(\text{odd/even})}(t, r_*^{\text{in}} + \Delta r_*), \end{aligned} \quad (3.4)$$

$$\begin{aligned} \Psi_{lm}^{(\text{odd/even})}(t + \Delta t, r_*^{\text{out}}) &= \left(1 - \frac{\Delta t}{\Delta r_*}\right) \Psi_{lm}^{(\text{odd/even})}(t, r_*^{\text{out}}) \\ &+ \frac{\Delta t}{\Delta r_*} \Psi_{lm}^{(\text{odd/even})}(t, r_*^{\text{out}} - \Delta r_*), \end{aligned} \quad (3.5)$$

where Δt and Δr_* are the step-size for time and space respectively. Note that we apply the first order finite differencing scheme in both space and time to the boundary conditions.

Although the initial condition we choose (Eq. [3.1]) is somewhat artificial, the particle motion is unaffected by gravitational radiation in our test particle approximation, and hence, after a certain evolution time, the radial wave function should converge into an appropriate solution. Therefore, we simply ignore the early stage of the evolution throughout this paper.

We should carefully deal with the delta function $\delta(r - \hat{R})$, which appears in the source term [Eq. (2.7)]. One treatment is to approximate the delta function to a step function that only covers one grid cell in the null coordinates [24, 27]. The other is to adopt, as we do here, an approximate function to describe a delta function, which appears in the source term, as [39]

$$\delta(r - \hat{R}) = \frac{1}{\sqrt{\pi}\sigma} \exp\left[-\frac{(r - \hat{R})^2}{\sigma^2}\right], \quad (3.6)$$

where σ is a standard deviation parameter. Note that Eq. (3.6) becomes exactly a delta function in the limit of $\sigma \rightarrow 0$.

We solve Eq. (2.7) in second order accuracy in space and time with the scheme based on two times iterated Crank-Nicholson method [52, 53]. We set the computational grid as $-1000M \leq r_* \leq R_{\text{obs}} + 2000M$, where R_{obs} is the location of the observer in the equatorial plane. We also set the step-size for space and time as $\Delta r_* = 1.0M$ and $\Delta t = 0.5 \times \Delta r_*$, which satisfies the Courant condition. Although we vary the location of the inner boundary $r_* \leq -1000M$, the difference of gravitational wave amplitude is within the round-off error.

We set the standard deviation parameter σ as $\sigma = \Delta r_*$. When σ is less than Δr_* , it is not certain to specify the location of a test particle due to the less spatial grid resolution, and therefore we discard such region. More concrete examinations of the dependence of σ on the circular and free fall orbits are discussed in the next two subsections.

A. Circular orbits

We compute the radial wave function from a test particle in a circular orbit at $R_c = 10M$ in Fig. 1, where R_c is the radius of the orbit. We set the standard deviation parameter as $\sigma = 0.1M$ and set the location of the observer at $R_{\text{obs}} = 2000M$. We only show the $l = m = 2$ mode, which is the dominant one for the observer in the equatorial plane. We find a burst in the early stage of the evolution, which comes from the inappropriate initial condition we imposed (Eq. [3.1]). Since the source term of Eq. (2.7) is unaffected by our initial condition, we simply ignore the unphysical burst in the wave function.

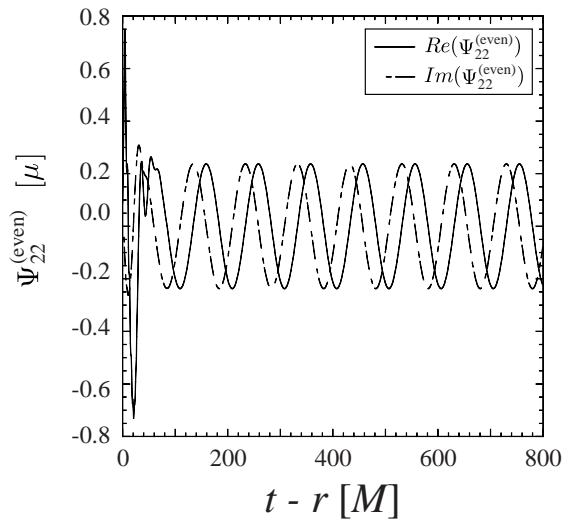


FIG. 1: Radial wave function of a test particle in a circular orbit at $R_c = 10M$. We only show the $l = m = 2$ mode, which is the dominant mode according to the observer in the equatorial plane at $R_{\text{obs}} = 2000M$. We set the standard deviation parameter as $\sigma = 0.1M$. Solid and dash-dotted lines represent real and imaginary parts of the radial wave function, respectively.

We vary the location of the observer R_{obs} to investigate the radius which is numerically regarded as infinity in Fig. 2. We only compute $l = m = 2$ mode, and vary the standard deviation parameter σ . It is clearly shown in Fig. 2 that the amplitude becomes almost constant when $R_{\text{obs}} \geq 2000M$, irrespective of the standard deviation parameter σ . Hereafter, we set the location of the observer at $R_{\text{obs}} \geq 2000M$.

We compare our numerical results with the ones of 5.5 post-Newtonian expansion [50] at two different radii,

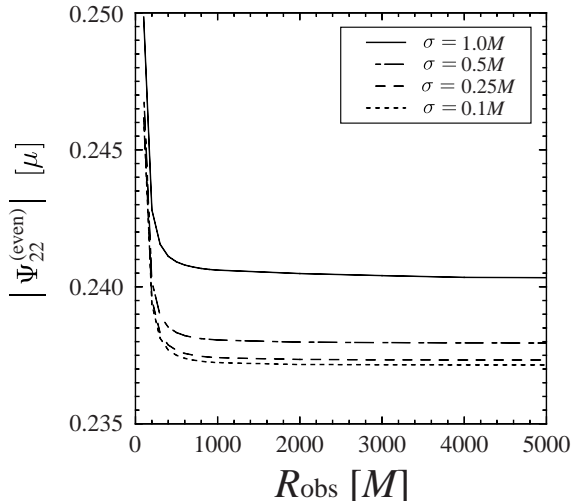


FIG. 2: The amplitude of the radial wave function as a function of the location of the observer R_{obs} . We only show the $l = m = 2$ mode. Solid, dash-dotted, dashed, dotted lines denote the standard deviation parameters $\sigma = 1.0M$, $0.5M$, $0.25M$, $0.1M$, respectively.

i.e., $R_c = 7M$ and $10M$. The energy flux of gravitational waves $(dE_{\text{gw}}/dt)^{(\text{PN})}$ from the analytical calculation (Eq. [3.1] of Ref. [50]) is that

$$\left(\frac{dE_{\text{gw}}}{dt}\right)^{(\text{PN})} = \begin{cases} 3.92 \times 10^{-5}(\mu/M)^2 & \text{for } R_c = 7M. \\ 6.13 \times 10^{-5}(\mu/M)^2 & \text{for } R_c = 10M. \end{cases} \quad (3.7)$$

Our energy flux for four different standard deviation parameters σ at $R_{\text{obs}} = 2000M$ is summarized in Table I. We sum up the index of the spherical harmonics l from 2 to 6. From Table I, we find that the deviation from the results of 5.5 post-Newtonian expansion becomes small when the standard deviation parameter σ becomes small. It is certainly true that this difference disappears within the limit of $\sigma \rightarrow 0$. We therefore conclude that for a circular orbit our code has good accuracy for $\sigma \lesssim 0.5M$ within the relative error of few percent in the energy flux.

We also mention the convergence order of our code. Since we use finite differencing scheme and approximate the delta function, there are two parameters σ and Δr_* for investigating the convergence order.

First we fix σ as $0.5M$ and varies Δr_* between $0.1M$ and $0.5M$. The energy flux (dE_{gw}/dt) at $R_c = 10M$ are $6.17 \times 10^{-5}[\mu^2/M^2]$ for $\Delta r_* = 0.1M$, $6.17 \times 10^{-5}[\mu^2/M^2]$ for $\Delta r_* = 0.2M$ (relative error from the energy flux of $\Delta r_* = 0.1M$ is 0.07%), $6.19 \times 10^{-5}[\mu^2/M^2]$ for $\Delta r_* = 0.4M$ (relative error 0.35%), and $6.20 \times 10^{-5}[\mu^2/M^2]$ for $\Delta r_* = 0.5M$ (relative error 0.56%). Therefore our code roughly has second order convergence in space, which is consistent with our second order finite differencing scheme. Next we fix the relationship $\sigma = \Delta r_*$ and varies

TABLE I: Comparison of our numerical results with the results of 5.5 post-Newtonian expansion (Eq. [3.7]).

R_c^a	σ^b	dE_{gw}/dt [μ^2/M^2] ^c	relative error [%]
7M	1.00M	4.15×10^{-5}	5.87
7M	0.50M	4.04×10^{-5}	3.06
7M	0.25M	4.01×10^{-5}	2.30
7M	0.10M	4.00×10^{-5}	2.04
10M	1.00M	6.35×10^{-5}	3.59
10M	0.50M	6.20×10^{-5}	1.14
10M	0.25M	6.16×10^{-5}	0.489
10M	0.10M	6.15×10^{-5}	0.326

^a R_c : Radius of the orbit

^b σ : Standard deviation parameter

^c dE_{gw}/dt : Energy flux of gravitational waves

σ between $0.1M$ and $1.0M$. Roughly speaking our code has first order convergence in σ , since the relative error in Table I decreases one half as σ becomes one half.

B. Free fall orbits

Next we compute gravitational waves from a test particle falling into a Schwarzschild black hole. We show the radial wave function of $l = m = 2$ mode at $R_{\text{obs}} = 7000M$ in Fig. 3. Instead of following the geodesics of a particle from infinity, we put an in-fall velocity at $r = r_{\text{int}}$ of $v \equiv dr_*/dt = -\sqrt{2M/r_{\text{int}}}$ derived from Eqs. (2.4) and (2.5). We also vary the initial radius of the test particle r_{int} in the range of $200M \leq r_{\text{int}} \leq 3000M$, and find that the total amount of radiated energy is in the relative error range of 0.001%. The radiated energy is determined by the integration of Eq. (2.23) in the range of $1600M \lesssim t - r \lesssim 3000M$ in Fig. 3. We set the spatial grid size $\Delta r_* = \sigma$, as we mentioned before. We show our convergence test of the ringing tail, varying Δr_* in Table II. We find that our computation has a convergence when we take $\sigma < 0.25M$. The resonance frequency agrees with the early results of Sasaki and Nakamura [54] ($M\omega \approx 0.30$), which corresponds to the frequency of the quasinormal mode of a Schwarzschild black hole.

TABLE II: Resonance frequencies of the quasi-normal ringing for some values of Δr_* and σ .

Δr_*	σ	$M\omega$
0.10M	0.10M	0.31
0.25M	0.25M	0.30
0.50M	0.50M	0.29
1.00M	1.00M	0.20

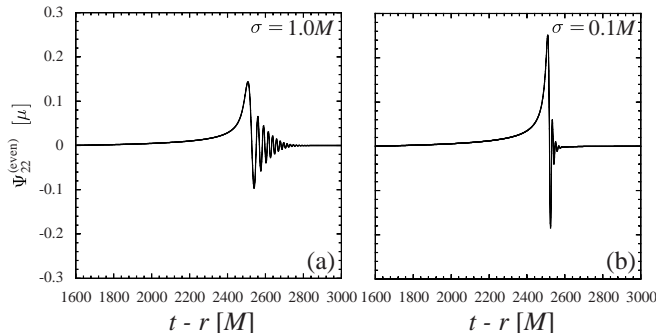


FIG. 3: Radial wave function of a test particle falling radially into a Schwarzschild black hole at $R_{\text{obs}} = 7000M$. We only show the $l = m = 2$ mode. The standard deviation parameters σ are (a) $1.0M$ and (b) $0.1M$, respectively. The parameters of oscillation frequency and the damping rate of the ringing tail are $(M\omega, M/\tau) =$ (a) $(0.199, 0.015)$, (b) $(0.314, 0.063)$, respectively.

TABLE III: Comparison of our numerical results with the results of a free fall orbit ($l = 2$ mode) [51].

R_{obs}	σ	$E_{\text{gw}} [\mu^2/M]$	relative error [%]
$5000M$	$1.00M$	4.94×10^{-3}	46.3
$5000M$	$0.50M$	8.38×10^{-3}	8.91
$5000M$	$0.25M$	8.78×10^{-3}	4.57
$5000M$	$0.10M$	8.96×10^{-3}	2.61
$7000M$	$1.00M$	4.17×10^{-3}	54.7
$7000M$	$0.50M$	7.94×10^{-3}	13.7
$7000M$	$0.25M$	8.71×10^{-3}	5.33
$7000M$	$0.10M$	8.95×10^{-3}	2.72

We compare our result with well-known one calculated in a frequency domain [51]. The radiated energy E_{gw} for the $l = 2$ mode is $E_{\text{gw}} = 9.2 \times 10^{-3}(\mu^2/M)$ in Ref. [51]. Our results are summarized in Table III. We have the same behavior as in the case of a circular orbit that the error is small as the standard deviation parameter becomes small. However, the relative error is larger than in the case of a circular orbit because a particle moves close to the black hole horizon, where the gravitational field is strong.

We also investigate the convergence order of our code in the free fall orbit. First we fix σ as $0.5M$ and varies Δr_* between $0.1M$ and $0.5M$. The radiated energy E_{gw} at $R_{\text{obs}} = 7000M$ are $9.65 \times 10^{-3}[\mu^2/M]$ for $\Delta r_* = 0.1M$, $9.54 \times 10^{-3}[\mu^2/M]$ for $\Delta r_* = 0.2M$ (relative error from the radiated energy of $\Delta r_* = 0.1M$ is 1.17%), $8.70 \times 10^{-3}[\mu^2/M]$ for $\Delta r_* = 0.4M$ (relative error 9.92%), and $7.94 \times 10^{-3}[\mu^2/M]$ for $\Delta r_* = 0.5M$ (relative

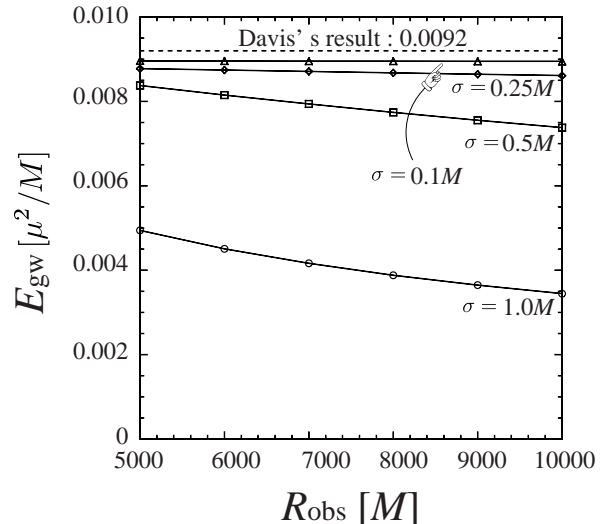


FIG. 4: Radiated energy of gravitational waves from a radially in-falling particle into a Schwarzschild black hole for the $l = 2$ mode. Circle, square, diamond, and triangle denote $\sigma = 1.0M, 0.5M, 0.25M$, and $0.1M$, respectively. Dotted line represents the numerical result of Ref. [51].

error 17.7%). Therefore our code has second order convergence in space. Next we fix the relationship $\sigma = \Delta r_*$ and varies σ between $0.1M$ and $1M$. Roughly speaking our code has a first order convergence in σ , since the relative error in Table III decreases one half as σ becomes one half. Note that the case $\sigma = 1.0M$ may be out of the convergence region.

We also set the observer quite far from the source in order to distinguish easily between the unphysical burst and the physical waveform. In fact, we integrate to compute the radiated energy in the range of $1600M < t-r_* < 3000M$. Note that the radiated energy is irrespective of the variation of the range of integration. In Fig. 4, we also show the dependence of the $l = 2$ mode E_{gw} on the location of the observer R_{obs} . We set the observer as $R_{\text{obs}} > 5000M$ since the inappropriate initial condition disturbs the burst of the waveform. From Fig. 4, we find that the total radiated energy for $\sigma = 1.0M$ and $0.5M$ are quite different from that found by Davis *et al.* [51] and this is irrespective of the location of the observer. The waveform with a large standard deviation parameter does not represent the quasi-normal ringing from a point particle.

From the comparison of our two numerical results with the two cases, we confirm that our code has an ability to handle gravitational waves from a particle in a free fall orbit and in a bounded orbit. The convergence order of our code is first order in σ and second order in Δr_* . We also find that we should set the parameter sets as $R_{\text{obs}} \geq 5000M$ and $\sigma \leq 0.25M$.

IV. GRAVITATIONAL WAVE FROM A DUST DISK

A. Construction of a dust disk

Here we explain our method for constructing a dust disk in Schwarzschild spacetime. We make five assumptions for constructing a dust disk as follows:

1. A disk has no self-interaction with each component; namely, a disk is composed of test particles.
2. A disk is thin so that the only components are located in the equatorial plane of a Schwarzschild black hole.
3. The density distribution for each radius of the disk is uniform so that it is considered as a uniform ring for each radius.
4. Each radius of the ring has a Keplerian orbit, that is to say, a circular orbit.
5. A disk is dynamically and radially stable.

From Assumption 5, our disk is only located outwards of the innermost stable circular orbit of a test particle in Schwarzschild spacetime. We show a brief picture of our disk in Fig. 5. Note that the disk is composed of test particles (from Assumption 1) in a circular orbit at each radius. Since we have a symmetry in the azimuthal direction of the particle motion, we can construct a ring from test particles using Assumption 3. Then, we compose a disk from rings.

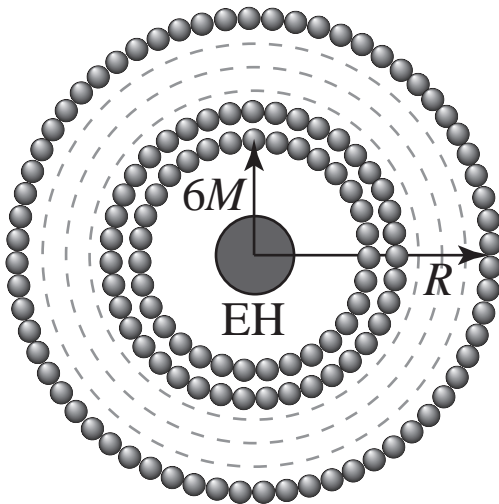


FIG. 5: Illustration of our disk composed of test particles in a Schwarzschild black hole. EH and R represent the event horizon and the outermost radius of the disk, respectively.

We regard the mass distribution per unit width of the disk at radius r as $m(r)$ given by

$$m(r) = 2\pi C\mu r^{1-n}, \quad (4.1)$$

where C , μ , and n represent the normalization constant that has a dimension of r^{n-2} , the rest mass of a test particle, and the factor of the mass distribution, respectively. Note that $n = 0$ denotes the constant mass density distribution of the disk. The total mass of the disk μ_{disk} is

$$\begin{aligned} \mu_{\text{disk}} &= \int_{6M}^R dr m(r) \\ &= \begin{cases} \frac{2}{2-n}\pi C\mu[R^{2-n} - (6M)^{2-n}] & (n \neq 2), \\ 2\pi C\mu[\ln(R/6M) - \ln 6] & (n = 2). \end{cases} \end{aligned} \quad (4.2)$$

In order to construct a disk numerically from a ring, we set each ring at the location which satisfies the energy

$$\tilde{E}_p^j = \tilde{E}_p^1 + \frac{j-1}{N_d-1}(\tilde{E}_p^{N_d} - \tilde{E}_p^1) \quad (j = 1, \dots, N_d), \quad (4.3)$$

where \tilde{E}_p^1 is the energy at $r = 6M$, $\tilde{E}_p^{N_d}$ is the energy at $r = R$, R is the radius of the disk, and N_d is the number of the rings.

In order to initiate the radial motion of a dust disk, we slightly deplete the angular momentum of each ring. Since we maintain the energy conserved during the depletion, we still follow the geodesic equation for a ring after the depletion.

B. Gravitational wave from a dust disk

Since we neglect the interaction between each component of the disk, gravitational waves emitted from the disk are obtained by superposing the waves emitted from each ring. For each gravitational wave emitted from each ring, we impose the same initial condition (Eq. [3.1]) and the same boundary condition (Eqs. [3.2] and [3.3]) as we used for the case of a test particle. In order to avoid the wave reflection at the boundary after a long evolution, we take the spatial grid as $-5000M < r_* \leq 10000M$. We also set the observer at $R_{\text{obs}} = 5000M$. The radial wave function of gravitational waves $\Psi_l^{(\text{disk})}$ is given by

$$\Psi_l^{(\text{disk})}(t, r) = \frac{1}{\mu_{\text{disk}}} \int_{6M}^R dr_0 m(r_0) \Psi_{l_0}^{(\text{odd/even})} \Big|_{r(0)=r_0}, \quad (4.4)$$

where r_0 represents the radius of the ring at $t = 0$. Only the $m = 0$ mode contributes to the gravitational waves from the ring due to its axisymmetric nature, where m is an index of spherical harmonics Y_{lm} . Therefore the amplitude of the gravitational wave is zero until the angular

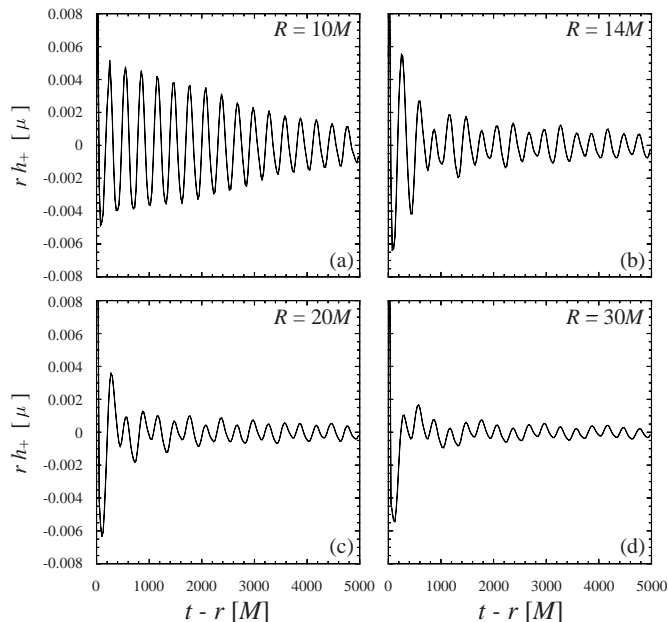


FIG. 6: Gravitational waveform from a dust disk at $R_{\text{obs}} = 5000M$ in the equatorial plane with constant density for four different disk radii, i.e., $R =$ (a) $10M$, (b) $14M$, (c) $20M$, and (d) $30M$.

momentum is depleted. We only take the $l = 2$ mode into consideration because it is the dominant mode for the observer in the equatorial plane. In this paper we consider only radial mode due to $m = 0$. However the radial mode has a fundamental physics and there is also in a realistic situation. Thus it is considered that we can extract some important evidence by this analysis.

We define the power spectrum of the gravitational waveform as

$$P(\omega) = \lim_{T \rightarrow \infty} \frac{1}{T} \left| \int_{-T/2}^{T/2} [h_+(t) - ih_\times(t)] e^{-i\omega t} dt \right|^2, \quad (4.5)$$

where ω is a frequency. In our computation, we choose as large a T as possible, namely $T = 4000M$, assuming that the phase difference apart from the periodic waves at the edge of the integration should be negligible. Note that we do not even integrate one long period of the wave in Fig. 6 (a) and Fig. 9 (a) (b) (c). The valid frequency range of the power spectrum is several $\times (2\pi/T) \lesssim \omega$, namely $0.005 \lesssim M\omega$, in all our computations. Hereafter we calculate the gravitational waves with $\Delta r_* = \sigma = 0.25M$ and $\Delta t = 0.5 \times \Delta r_*$.

1. Constant rest mass density distribution

First we assume that the rest mass density distribution of the disk is uniform, namely $n = 0$ in Eq. (4.1). We vary the outermost radius of the disk as $R = 10M$, $14M$, $20M$, and $30M$. We deplete 1% of the angular

momentum of each ring at $(t - r)/M = 0$ to initiate the radial motion. As a matter of fact, the innermost radially stable fragments of the disk approach $r \sim 7.85M$. We show the gravitational waveform from a dust disk in Fig. 6. Since a uniform ring with a circular orbit retains an axisymmetric nature in the system, the system does not emit gravitational waves before the depletion.

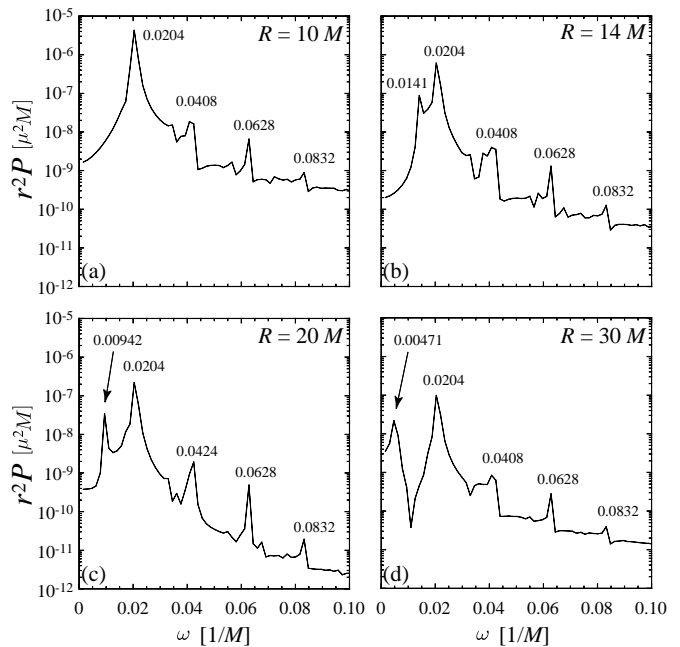


FIG. 7: The power spectrum of the gravitational waveform in Fig. 6. We extract the time range of $1000M \lesssim t - r \lesssim 5000M$ to compute the power spectrum. The radius of the disk R is (a) $10M$, (b) $14M$, (c) $20M$, (d) $30M$. The values correspond to the peaks of the spectrum.

We choose $N_d = 50, 100, 175,$ and 300 for $R = 10M, 14M, 20M,$ and $30M$, respectively, so that the step-size of the integration in Eq. (4.4) should be the same. As the distance between the closest two radii of the components at $t = 0$ is $0.035M \sim 0.26M$ depending on the radius, the components have sufficient numbers of particles to compose a disk. The first burst in the waveform is regarded as an inappropriate choice of the initial condition, as we mentioned in Sec. III.

Since the waveforms (except for the disk with $R = 10M$) are very similar to each other, it is difficult to obtain information on the disk solely from the waveforms. However, we find that there is a clear difference in the power spectrum of a gravitational waveform, varying the radius of the disk (Fig. 7). Note that the spectrum of Fig. 7 is calculated from the waveforms of Fig. 6. To construct a power spectrum, we take the data set of a waveform in the range of $1000M \lesssim t - r \lesssim 5000M$. The value in Fig. 7 corresponds to the frequency $M\omega$ of each

TABLE IV: Relationship between the initial radius of the ring and the characteristic frequency of gravitational waves from a ring.

$R_{\text{ring}}^c [M]$	$M\omega_{\text{gw}}^d$
8.0	0.0204
10.0	0.0204
14.0	0.0141
20.0	0.00942
30.0	0.00471

^c R_{ring} : Radius of the ring

^d $M\omega_{\text{gw}}$: Characteristic frequency of gravitational waves from a ring induced by 1% depletion of the angular momentum.

peak. From these power spectra, the peak frequencies are almost the same, irrespective of the disk radius. However, for $R = 14M$, $20M$, and $30M$ there is another peak frequency, which is lower than the frequency of the first peak in the case where $R = 10M$.

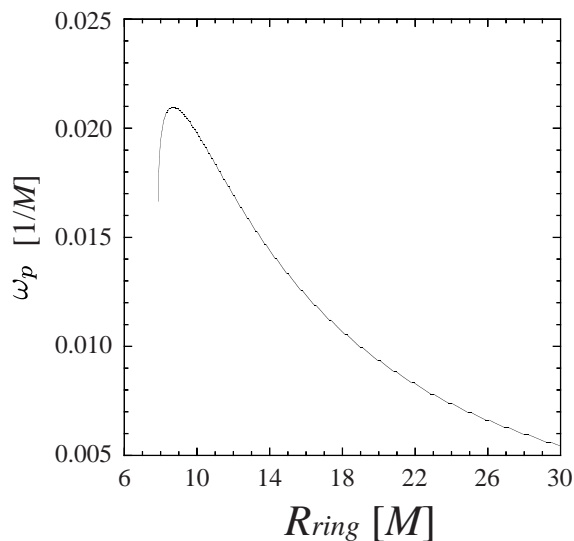


FIG. 8: Radial frequency ω_p of the particle as a function of initial location R_{ring} .

In order to understand the peak frequencies in the power spectra, we calculate the characteristic frequency of a particle around a Schwarzschild black hole. We summarize the characteristic frequencies of gravitational waves from a test particle with 1% depletion of the angular momentum from a circular orbit in Table IV. From Fig. 7 and Table IV, the peak frequency $M\omega = 0.0204$, which appears in all disk models, corresponds to the characteristic frequency of a ring ω_{gw} of $R_{\text{ring}} = 8M$ and $10M$, and another peak frequency lower than $M\omega =$

0.0204 corresponds to the characteristic frequency of a particle at the outermost edge of the disk. Note that the peak frequencies above $M\omega = 0.0204$ correspond to the higher-order frequency of $M\omega = 0.0204$. In fact, the corresponding frequencies have the following rule: $0.0408 = 0.0204 \times 2$, $0.0628 \approx 0.0204 \times 3$, $0.0832 \approx 0.0204 \times 4$.

The peak of the frequency below $M\omega = 0.0204$ comes from the ring at the outer edge of the disk, and the peak at $M\omega = 0.0204$ comes from the ring at the inner edge of the disk. The reason for no peak at the frequency below $M\omega = 0.0204$ of a disk with $R = 10M$ is that the frequency corresponding to $R = 10M$ is the same as that of the peak at $M\omega = 0.0204$. The phase cancellation effect plays a role in the emission of gravitational waves from the rings between the two edges of the disk. Therefore, it is possible to determine the radius of a dust disk from the power spectrum if the disk radius is $\gtrsim 12M$.

The characteristic frequency ω_{gw} coincides with the radial frequency ω_p of a particle at $r = R_{\text{ring}}$ due to the axisymmetric motion of the disk that corresponds to the $m = 0$ mode. In Fig. 8, we plot the relation between the radial frequencies ω_p of the particle at R_{ring} and initial particle radius R_{ring} . Note that we deplete 1% of the angular momentum of the ring to initiate the radial motion. Since our frequency resolution is $M\Delta\omega \approx 0.005$ as we mentioned before, the frequency ω_p and ω_{gw} have a good correspondence. As mentioned above, because a peak corresponds to ω_{gw} at $R_{\text{ring}} = R$ in the power spectrum of gravitational waves, it is expected that we can determine the radius of a dust disk using the relation between ω_p and R_{ring} . The quasi-normal ringing in the waveform represents the character of black hole; we can determine the character of the central black hole from the ringing. In a dust disk system, however, we cannot find the quasi-normal ringing in the waveform because there is a continuous inflow of fragments into a Schwarzschild black hole. Therefore the ringing is canceled by the different phase of the wave generated by each inflow fragment.

2. Non-constant rest mass density distribution

Next we consider the non-constant mass density distribution of a dust disk, which means that the rest mass density of the outermost edge of the disk is lower than that of the innermost edge, i.e., $n > 0$. In Fig. 9, we show a waveform from a dust disk with $R = 10M$ and $R = 30M$ for $n = 0.5, 1.0$, and 2.0 , respectively. For a disk with $R = 10M$, the waveform does not strongly depend on the distribution. For the disk models with $R = 30M$, the waveforms approach those of the disk models with $R = 10M$ as n becomes larger. Therefore it is also difficult to obtain information on the disk from the observational waveforms. However, in the power spectra (Fig. 10), the frequency corresponds to the peak having

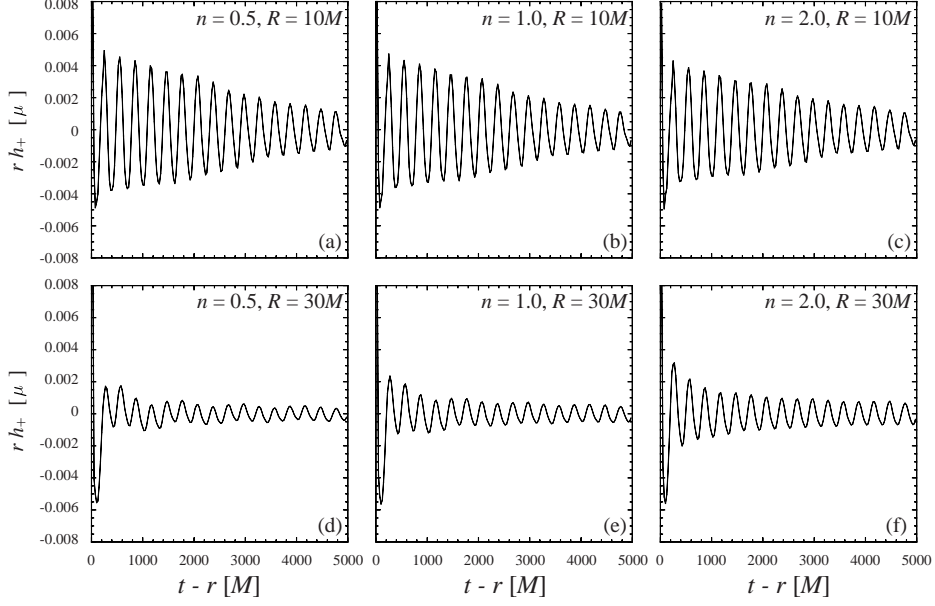


FIG. 9: Gravitational waveform of a dust disk as a function of $t-r$. The parameters (n, R) are (a) $(0.5, 10M)$, (b) $(1.0, 10M)$, (c) $(2.0, 10M)$, (d) $(0.5, 30M)$, (e) $(1.0, 30M)$, (f) $(2.0, 30M)$. We set the observer in the equatorial plane at $R_{\text{obs}} = 5000M$.

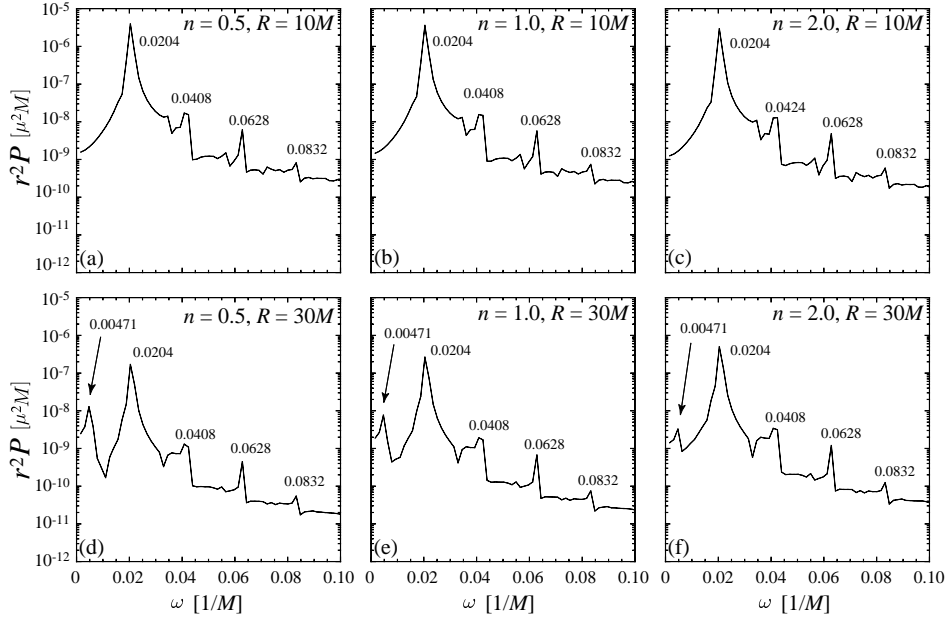


FIG. 10: Power spectrum of gravitational waveforms in Fig. 9. We extract the time range of $1000M \lesssim t-r \lesssim 5000M$ to compute the power spectrum. The values correspond to the peaks of the spectrum.

the same feature as the one in the case where $n = 0$. Thus, the peak frequencies in the power spectrum correspond to those of gravitational waves from a ring at $R_{\text{ring}} = R$ and at the inner region of the disk. Therefore, we conclude that we can determine the radius of the disk irrespective of the density distribution using the power spectrum of gravitational waves.

3. Different type of angular momentum depletion

Here we show our result based on a different type of angular momentum depletion of test particles whether our statement largely depends on the type of depletion.

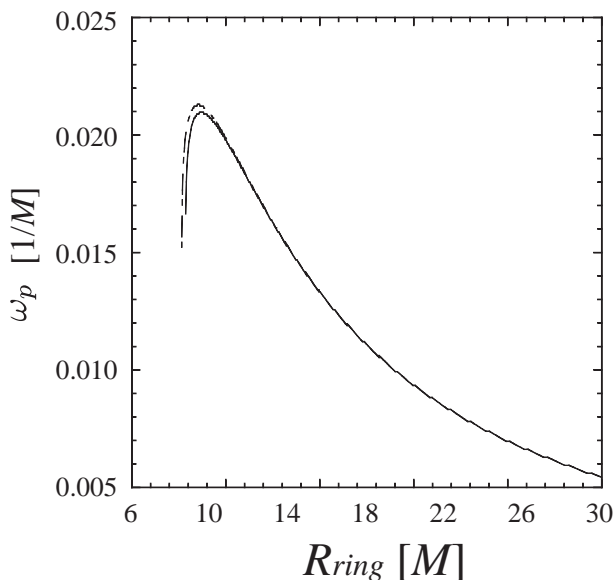


FIG. 11: Radial frequency ω_p of the particle as a function of initial location R_{ring} . Dash line corresponds to ω_p of the particle with a different angular momentum depletion (Eq. [4.6]) and the solid line with the same angular momentum depletion as Fig. 8.

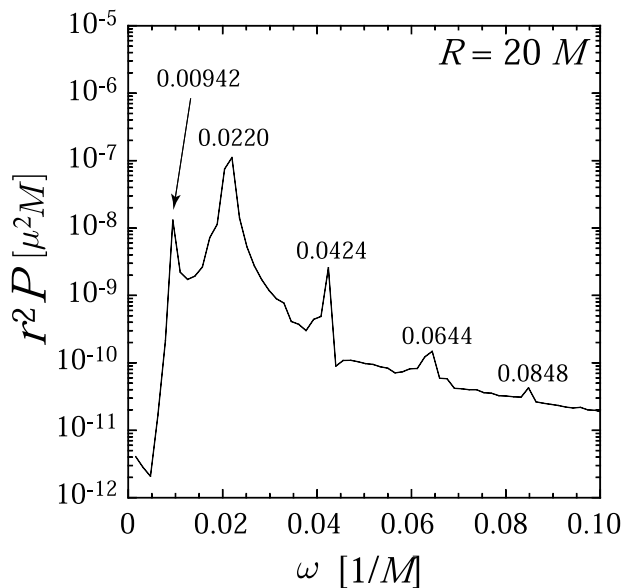


FIG. 12: Power spectrum of gravitational waves from a dust disk with a different type of angular momentum depletion (See Eq. [4.6]). We choose the density profile of the disk as uniform, with the disk radius $R = 20M$. The values in the figure correspond to the peaks of spectrum.

We deplete the angular momentum of the fragments in the following manner:

$$\frac{\Delta L_p}{L_p} = \frac{6M}{r} \times 10^{-2}. \quad (4.6)$$

The gravitational wave spectrum from the constant rest-mass density distribution is shown in Fig. 12. Although the orbit of each fragments has been changed (the characteristic frequency is shown in Fig. 11), the peak frequencies in the power spectrum correspond to those of gravitational waves from a ring at $R_{\text{ring}} = R$ and at the inner region of the disk. Therefore, we can determine the radius of the disk in a different type of angular momentum depletion using the power spectrum of gravitational waves.

V. CONCLUSIONS

We study gravitational waves from a dust disk around a Schwarzschild black hole using a black hole perturbation approach in a time domain. We especially focus on whether we can obtain the radius of the disk from gravitational waves.

We find that it is difficult to obtain information on the dust disk only by the observational waveforms. However, it is possible to determine the radius of the disk using the power spectrum of gravitational waves, irrespective of its density distribution. Our conclusion is quite similar to the findings of Saijo and Nakamura [44, 45]. They claim that when a star is tidally disrupted by the central rotating black hole, we can determine the radius of the star from the spectrum of gravitational waves. In addition, there is also a peak corresponding to a frequency of gravitational waves from a particle located at the inner edge of the disk. Since the standard deviation of the inner edge of the disk from $R = 6M$ is a consequence of the radiated angular momentum, we could estimate the amount of radiation from the radius standard deviating from the innermost circular orbit. Although the detail disruption process requires 3D general relativistic calculation with the whole energy transport process, our statement from the simple model is still helpful to understand the disruption process by observing the gravitational wave spectrum.

We also mention the target of the gravitational wave source and its detectability. The typical frequency and the strength in our dust disk model are

$$f = \frac{\omega}{2\pi} = 6.59 \times 10^{-4} \left(\frac{10^6 M_\odot}{M} \right) \left(\frac{M\omega}{0.0204} \right), \quad (5.1)$$

$$h = 4.78 \times 10^{-23} \left(\frac{1\text{Mpc}}{r} \right) \left(\frac{M}{10^6 M_\odot} \right) \left(\frac{\mu/M}{10^{-6}} \right) \left(\frac{r h_+ / \mu}{0.001} \right). \quad (5.2)$$

Therefore it is possible to detect gravitational waves from a dust disk oscillating around a supermassive black hole by LISA.

We have only investigated the outermost radius of the disk up to $\sim 30M$ due to a limitation on computational time. However, our finding can be extrapolated into a more general astrophysical situation, such as the black hole formation phase of a supermassive star collapse. In

this phase, the collapse forms a supermassive black hole and a disk [55, 56], and the fragments of the disk could fall into the supermassive black hole due to some dissipative mechanism or instabilities of the fluid that lead to a different configuration. The interaction between each material components of the disk is considerably small for soft equation of state such as a supermassive star, the radial oscillation of the disk may take a dominant role in exciting a peak in the power spectrum of gravitational waves. Therefore it could be one source generation scenario of gravitational waves useful for determining the size of the disk.

Acknowledgments

It is our pleasure to thank Nobuyuki Kanda and Hideyuki Tagoshi for their valuable advice. HS gratefully

acknowledges helpful discussion with Shijun Yoshida. We also thank Peter Musolf for his careful reading of our manuscript. This work was supported in part by the Marie Curie Incoming International Fellowships (MIF1-CT-2005-021979), by MEXT Grant-in-Aid for young scientists (No. 200200927), and by the PPARC grant (PPA/G/S/2002/00531) at the University of Southampton. Numerical computations were carried out on the Pentium-4 type machines of the Astrophysics and Cosmology Group, Waseda University, and of the Yukawa Institute for Theoretical Physics, Kyoto University.

-
- [1] B. C. Barish, in *Proceedings of the 17th International Conference on General Relativity and Gravitation*, edited by P. Florides, B. Nolan and A. Ottewill (World Scientific, New Jersey, 2005), p. 24.
- [2] C. Cutler and K. S. Thorne, in *Proceedings of the 16th International Conference of General Relativity and Gravitation*, edited by N. T. Bishop and S. D. Maharaj (World Scientific, New Jersey, 2002), p. 72.
- [3] J. Kormendy, in *Carnegie Observatories Centennial Symposium. 1: Coevolution of Black Holes and Galaxies*, edited by L. C. Ho (Cambridge Univ. Press, Cambridge, 2004), p. 1.
- [4] F. Melia and H. Falcke, *Annu. Rev. Astron. Astrophys.* **39**, 309 (2001).
- [5] J. M. Jackson, N. Geis, R. Genzel, A. I. Harris, S. Madden, A. Poglitsch, G. J. Stacey, and C. H. Townes, *Astrophys. J.* **402**, 173 (1993).
- [6] S. Komossa, J. Halpern, N. Schartel, G. Hasinger, M. Santos-Lleo, and P. Predehl, *Astrophys. J.* **603**, L17 (2004).
- [7] J. P. Halpern, S. Gezari, and S. Komossa, *Astrophys. J.* **604**, 572 (2004).
- [8] C. R. Evans and C. S. Kochanek, *Astrophys. J.* **346**, L13 (1989).
- [9] B. Carter and J. -P. Luminet, *Astron. Astrophys.* **121**, 97 (1983).
- [10] B. Carter and J. -P. Luminet, *Mon. Not. R. Astron. Soc.* **212**, 23 (1985).
- [11] A. Khokhlov, I. D. Novikov, and C. J. Pethick, *Astrophys. J.* **418**, 163 (1993); **418**, 181 (1993).
- [12] J. A. Marck, A. Lioure, and S. Bonazzola, *Astron. Astrophys.* **306**, 666 (1996).
- [13] S. Ayal, M. Livio, and T. Piran, *Astrophys. J.* **545**, 772 (2000).
- [14] P. Laguna, W. A. Miller, W. H. Zurek, and M. B. Davies, *Astrophys. J.* **410**, L83 (1993).
- [15] B. Mashhoon, *Astrophys. J.* **197**, 705 (1975).
- [16] L. G. Fishbone, *Astrophys. J.* **185**, 43 (1973).
- [17] V. P. Frolov, A. M. Khokhlov, I. D. Novikov, and C. J. Pehick, *Astrophys. J.* **432**, 680 (1994).
- [18] M. Shibata, *Prog. Theor. Phys.* **96**, 917 (1996).
- [19] P. Diener, V. P. Frolov, A. M. Khokhlov, I. D. Novikov, and C. J. Pehick, *Astrophys. J.* **479**, 164 (1997).
- [20] L. G. Cannizo, H. M. Lee, and J. Goodman, *Astrophys. J.* **351**, 38 (1990).
- [21] M. Sasaki and H. Tagoshi, *Living Rev. Relativity* **6**, 6 (2003).
- [22] T. Nakamura, K. Oohara, and Y. Kojima, *Prog. Theor. Phys. Suppl.* **90**, Parts II and III (1987).
- [23] C. O. Lousto and R. H. Price, *Phys. Rev. D* **55**, 2124 (1997).
- [24] C. O. Lousto and R. H. Price, *Phys. Rev. D* **56**, 6439 (1997).
- [25] C. O. Lousto and R. H. Price, *Phys. Rev. D* **57**, 1073 (1998).
- [26] C. Gundlach, R. H. Price, and J. Pullin, *Phys. Rev. D* **49**, 883 (1994); **49**, 890 (1994).
- [27] K. Martel and E. Poisson, *Phys. Rev. D* **66**, 084001 (2002).
- [28] K. Martel, *Phys. Rev. D* **69**, 044025 (2004).
- [29] E. Poisson, *Phys. Rev. D* **70**, 084044 (2004).
- [30] A. Nagar, J. A. Font, O. Zanotti and R. De Pietri, *Phys. Rev. D* **72**, 024007 (2005).
- [31] W. Krivan, P. Laguna, P. Papadopoulos, and N. Andersson, *Phys. Rev. D* **56**, 3395 (1997).
- [32] R. López-Alemán, G. Khana, and J. Pullin, *Class. Quantum Grav.* **20**, 3259 (2003).
- [33] G. Khana, *Phys. Rev. D* **69**, 024016 (2004).
- [34] E. Pazos-Avalos and C. O. Lousto, *Phys. Rev. D* **72**, 084022 (2005).
- [35] N. Andersson and K. D. Kokkotas, *Phys. Rev. Lett.* **77**, 4134 (1996).
- [36] G. Allen, N. Andersson, K. D. Kokkotas, and B. F. Schutz, *Phys. Rev. D* **58**, 124012 (1998).
- [37] G. Allen, N. Andersson, K. D. Kokkotas, P. Laguna, J. A. Pullin, and J. Ruoff, *Phys. Rev. D* **60**, 104021 (1999).
- [38] J. Ruoff, *Phys. Rev. D* **63**, 064018 (2001).
- [39] J. Ruoff, P. Laguna, and J. Pullin, *Phys. Rev. D* **63**, 064019 (2001).

- [40] A. Nagar, G. Diaz, J. A. Pons and J. A. Font, Phys. Rev. D **69**, 124028 (2004).
- [41] J. Ruoff and K. D. Kokkotas, Mon. Not. R. Astron. Soc. **328**, 678 (2001).
- [42] J. Ruoff, A. Stavridis, and K. D. Kokkotas, Mon. Not. R. Astron. Soc. **332**, 676 (2002).
- [43] M. Vallisneri, Phys. Rev. Lett. **84**, 3519 (2000).
- [44] M. Saijo and T. Nakamura, Phys. Rev. Lett. **85**, 2665 (2000).
- [45] M. Saijo and T. Nakamura, Phys. Rev. D **63**, 064004 (2001).
- [46] T. Bogdanović, M. Eracleous, S. Mahadevan, S. Sigurdsson, and P. Laguna, Astrophys. J. **610**, 707 (2004).
- [47] S. Kobayashi, P. Laguna, E. S. Phinney, and P. Meszaros, Astrophys. J. **615**, 855 (2004).
- [48] T. Regge and J. A. Wheeler, Phys. Rev. **108**, 1063 (1957).
- [49] F. J. Zerilli, Phys. Rev. D **2**, 2141 (1970); Phys. Rev. Lett. **24**, 737 (1970).
- [50] T. Tanaka, H. Tagoshi, and M. Sasaki, Prog. Theor. Phys. **96**, 1087 (1996).
- [51] M. Davis, R. Ruffini, W. H. Press, and R. H. Price, Phys. Rev. Lett. **27**, 1466 (1971).
- [52] W. H. Press, B. P. Flannery, S. A. Teukolsky, and W. T. Vetterling, *Numerical Recipes in Fortran* (Cambridge Univ. Press, Cambridge, 1992), Chap. 19.2.
- [53] S. A. Teukolsky, Phys. Rev. D **61**, 087501 (2000).
- [54] M. Sasaki and T. Nakamura, Prog. Theor. Phys. **67**, 1788 (1982).
- [55] M. Saijo, T. W. Baumgarte, S. L. Shapiro, and M. Shibata, Astrophys. J. **569**, 349 (2002).
- [56] M. Shibata and S. L. Shapiro, Astrophys. J. **572**, L39 (2002).